

Structural and magnetic properties of cobalt ferrite nanoparticles synthesized by co-precipitation at increasing temperatures

Cite as: AIP Advances 8, 056303 (2018); <https://doi.org/10.1063/1.5006321>

Submitted: 24 September 2017 • Accepted: 17 October 2017 • Published Online: 07 December 2017

C. R. Stein,  M. T. S. Bezerra, G. H. A. Holanda, et al.

COLLECTIONS

Paper published as part of the special topic on [62nd Annual Conference on Magnetism and Magnetic Materials](#)



View Online



Export Citation



CrossMark

ARTICLES YOU MAY BE INTERESTED IN

[High temperature magnetic properties of cobalt ferrite nanoparticles](#)

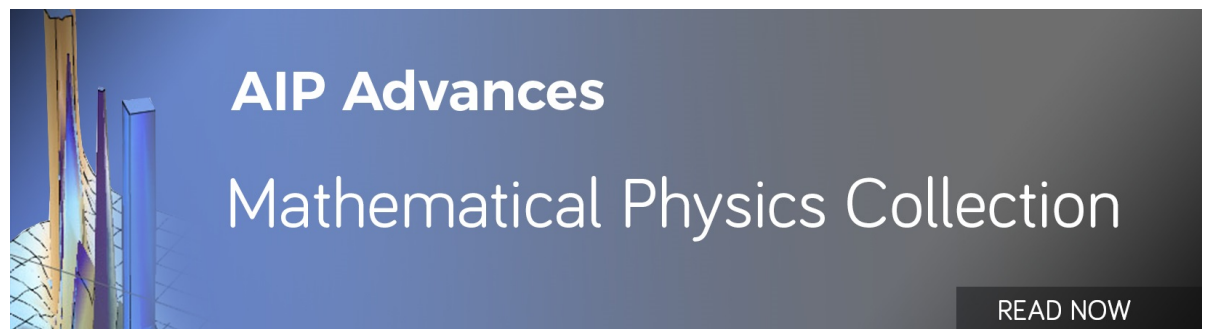
Applied Physics Letters **96**, 172505 (2010); <https://doi.org/10.1063/1.3422478>

[Magnetic and electrical properties of In doped cobalt ferrite nanoparticles](#)

Journal of Applied Physics **112**, 084321 (2012); <https://doi.org/10.1063/1.4759436>

[Structural, dielectric and magnetic properties of nickel substituted cobalt ferrite nanoparticles: Effect of nickel concentration](#)

AIP Advances **5**, 097166 (2015); <https://doi.org/10.1063/1.4931908>



AIP Advances
Mathematical Physics Collection

READ NOW

Structural and magnetic properties of cobalt ferrite nanoparticles synthesized by co-precipitation at increasing temperatures

C. R. Stein,^{1,2,a} M. T. S. Bezerra,¹ G. H. A. Holanda,¹ J. André-Filho,² and P. C. Morais^{2,3}

¹Federal Institute of Rondônia, Porto Velho RO 76820-441, Brazil

²University of Brasília, Institute of Physics, Brasília DF 70910-900, Brazil

³Anhui University, School of Chemistry and Chemical Engineering, Hefei 230601, China

(Presented 7 November 2017; received 24 September 2017; accepted 17 October 2017; published online 7 December 2017)

This study reports on the synthesis and characterization of cobalt ferrite (CoFe₂O₄) nanoparticles (NPs) synthesized by chemical co-precipitation in alkaline medium at increasing temperatures in the range of 27 °C to 100 °C. High-quality samples in the size range of 5 to 10 nm were produced using very low stirring speed (250 rpm) and moderate alkaline aqueous solution concentration (4.8 mol/L). Three samples were synthesized and characterized by x-ray diffraction (XRD) and room-temperature (RT) magnetization measurements. All samples present superparamagnetic (SPM) behavior at RT and Rietveld refinements confirm the inverse cubic spinel structure (space group Fd-3m (227)) with minor detectable impurity phase. As the synthesis temperature increases, structural parameters such as lattice constant and grain size change monotonically from 8.385 to 8.383 Å and from 5.8 to 7.4 nm, respectively. Likewise, as the synthesis temperature increases the NPs' magnetic moment and saturation magnetization increases monotonically from 2.6×10^3 to 16×10^3 μ_B and from 37 to 66 emu/g, respectively. The RT magnetization (M) versus applied field (H) curves were analyzed by the first-order Langevin function averaged out by a lognormal distribution function of magnetic moments. The excellent curve-fitting of the M versus H data is credited to a reduced particle-particle interaction due to both the SPM behavior and the existence of a surface amorphous shell layer (dead layer), the latter reducing systematically as the synthesis temperature increases. © 2017 Author(s). All article content, except where otherwise noted, is licensed under a Creative Commons Attribution (CC BY) license (<http://creativecommons.org/licenses/by/4.0/>). <https://doi.org/10.1063/1.5006321>

INTRODUCTION

Cobalt ferrite (CoFe₂O₄) nanoparticles (NPs) have attracted continuous interest over the last past decades due to many applications this nanomaterial has been connected with, to name a few magneto-optical devices,¹ contrast agent for MRI,² drug delivery systems,³ spintronics,⁴ and magnetohyperthermia.⁵ Reduced dimensionality of cobalt ferrite NPs shows differences in properties when compared to its bulk counterpart.⁶⁻⁸ Moreover, size modulation of the physicochemical properties of cobalt ferrite is a typical response in the nanosized regime, allowing for material engineering in order to meet different requirements while addressing applications.⁹ In addition to size and size dispersity,¹⁰ materials engineering regarding core-shell design,¹¹ shape,¹² crystallinity,^{13,14} surface decoration¹⁵ and hybrid derivatives¹⁶ opens up a wide variety of opportunities for basic studies as well as for development and innovation. Despite different synthesis routes of cobalt ferrite NPs already reported in the literature optimization of morphology and physicochemical properties is still

^aclever.stein@ifro.edu.br

far from being exhausted.^{17–19} In this study, we report on the synthesis, structural characterization and magnetic properties of cobalt ferrite NPs realized in different temperatures. Differently from a previous study,²⁰ we succeeded in fabricating high-quality CoFe_2O_4 NPs with modulating size in the range of 5 to 10 nm by reducing the stirring speed of the reaction medium by a factor of 40 while increasing the concentration of the added base only about thrice, thus representing a remarkable improvement for prospecting future up-scaling production.

EXPERIMENTAL

Co-precipitation in alkaline medium was used as the synthetic route to fabricate the CoFe_2O_4 NPs.^{21–24} In addition to be cost-effective this method of synthesis usually provides NPs with relative narrow size distribution.^{25,26} Hydrochloric acidic (HCl) aqueous solutions ($0.01 \text{ mol}\times\text{L}^{-1}$) containing Fe^{3+} and Co^{2+} ions prepared from hexahydrate chloride salts were mixed in stoichiometric 2:1 ($\text{Fe}^{3+}:\text{Co}^{2+}$) molar ratio under stirring (250 rpm) for 20 minutes, at different temperatures (30, 50, and 95 °C). Next, 50 mL of sodium hydroxide (NaOH) aqueous solution ($4.8 \text{ mol}\times\text{L}^{-1}$), pre-heated at the same temperature, was added into the reaction medium while keeping the same stirring speed (250 rpm) and temperature (30, 50, and 95 °C) for extra 30 minutes. The repeated synthesis protocol produced three different samples, namely CO30, CO50, and CO95. After synthesis, each product was naturally cooled down to room temperature and separated by magnetic decantation. The supernatant was disregarded and precipitate washed with water several times. The resulting slurries were dried at 40 °C in order to carry on structural and magnetic characterization. X-ray diffraction (XRD) was used to characterize the as-synthesized samples while providing estimative of the crystallite size. XRD data of all samples were recorded in a Shimadzu model XRD 6000 system using the Cu $K\alpha$ ($\lambda = 1.5418 \text{ \AA}$) line scanning in the range of $2\theta = 10 - 80^\circ$ at 2 degrees/minute. The average size of crystallite domains (D_{hkl}) (see Table II) was calculated using the Scherrer formula.²⁷ A SQUID MPMS 3 system (Quantum Design, San Diego California - USA) was used to collect the room-temperature hysteresis cycles in the range of $\pm 60 \text{ kOe}$.

RESULTS AND DISCUSSIONS

Lattice parameters and crystallite sizes have been assessed from the XRD data by means of the Rietveld refinement method using the DBWS 9411 program.²⁸ Figure 1 shows the XRD data of all prepared samples while crystallographic parameters obtained from the Rietveld refinement are collected in Table I. As criteria for quality of the Rietveld refinement the differential spectra are shown below each XRD spectra (see Fig. 1). Refinement of the XRD patterns show formation of a major spinel structure phase (CoFe_2O_4) with space group symmetry $\text{Fd-}3\text{m}(227)$ (JCPDS card no. 22-1086), accompanied by metallic iron as impurity. Structures in the differential spectrum shown in Fig. 1 account for the iron impurity, not exceeding $R_{\text{exp}} = 10\%$ in all samples, which is typically found in the literature for chemical co-precipitation route.²⁹ Our analyses show that cobalt and iron ions occupy the $8a$ and $16d$ Wyckoff positions at (0.5, 0.5, 0.5) and (0.125, 0.125, 0.125), respectively. Oxygen ions occupy the $32e$ Wyckoff position, with positional parameter x shown in the last column of Table I^{30,31} The data collected in Table I clearly show the systematic evolution of all crystalline parameters of the as-synthesized samples toward the standard values of bulk cobalt ferrite, as the synthesis temperature increases from 30 to 95 °C. This finding reveals the improvement on the crystalline quality of the as-synthesized samples as the synthesis temperature increases in the range of 27 to 100 °C, with positive impact on the magnetic properties as it will be discussed below.

The room-temperature magnetization (M) versus applied field (H) is shown in Fig. 2, where symbols are experimental data and solid lines represent the best curve-fitting according to Eqs. (1) and (2). Data presented in Fig. 2 show no room-temperature remanence or coercivity, thus indicating the superparamagnetic behavior of all synthesized CoFe_2O_4 NPs. Therefore, the first-order Langevin function (L), averaged out by the lognormal distribution function (f) of particle's magnetic

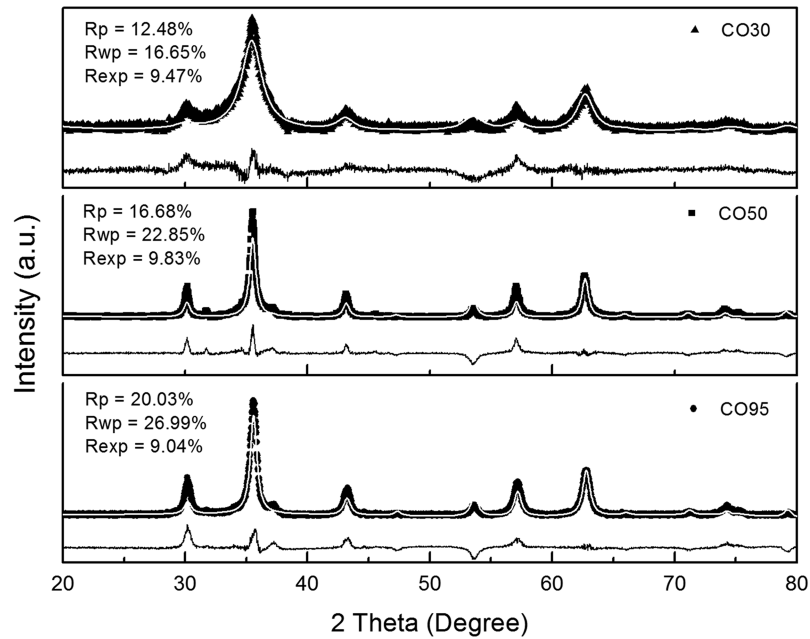


FIG. 1. Rietveld refinement of the x-ray powder diffraction pattern of samples CO30, CO50, and CO95. Rp, Rwp and Rexp stand for profile residual, weighted profile factor and profile expected, respectively. Differential spectrum is shown below each spectrum.

moment (μ), was used to fit the magnetization data and extract relevant parameters:

$$M(H, T) = M_s \int_{\mu_-}^{\mu_+} \mu L\left(\frac{\mu H}{k_B T}\right) f(\mu) d\mu, \quad (1)$$

where M_s is the sample's saturation magnetization, k_B the Boltzmann constant, and T the absolute temperature. The lognormal distribution function reads:

$$f(\mu) = \left(\frac{N}{\sigma_\mu \mu_0 \sqrt{2\pi}}\right) \exp\left\{-\left[\frac{\ln^2(\mu/\mu_0)}{2\sigma_\mu^2}\right]\right\}, \quad (2)$$

where N is the number of particles per cm^3 , μ_0 is the average magnetic moment, and σ_μ is the magnetic moment dispersity. In order to allow easy convergence while fitting the magnetization data values of μ_- and μ_+ in Eq. (1) were set in the range $0 < \mu < \infty$. Table II collects the parameters extracted from fitting the experimental data shown in Fig. 2. Worth mentioning that M_s increases systematically as the synthesis temperature increases in the range of 27 to 100 °C, following the crystallite size trends extracted from the analysis of the XRD data (see Table II). Actually, enhancement of the saturation magnetization (and average magnetic moment) is due to the increase of the average crystallite size plus improvement in crystallinity, both working to strengthen the long-range magnetic ordering. Moreover, Table II also shows a systematic reduction of the magnetic moment dispersity as the synthesis temperature increases, likely due the narrowing of the particle size

TABLE I. Lattice parameter (a), unit cell volume (V), x-ray mass density (ρ_{XRD}), and oxygen positional parameter (x). The last line collects the bulk ferrite cobalt data from JCPDS card no. 22-1086.

Samples	a (Å)	V (Å ³)	ρ_{XRD} (g/cm ³)	x (Å)
CO30	8.358±0.004	583.86±0.03	6.06±0.05	0.791±0.002
CO50	8.365±0.002	585.33±0.02	6.03±0.03	0.831±0.002
CO95	8.383±0.002	589.11±0.02	6.01±0.03	0.868±0.002
JCPDS card no. 22-1086	8.3919	590.99	5.274	0.925

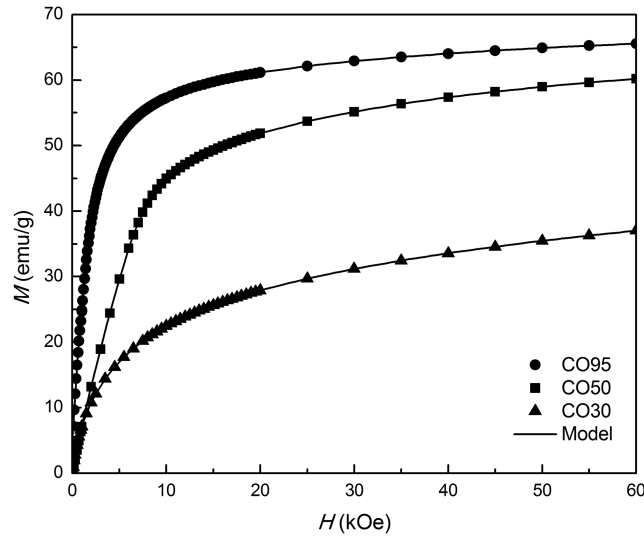


FIG. 2. Room-temperature magnetization data (symbols) of three samples (CO30, CO50, and CO95) and the corresponding curve fitting (solid lines) using a model picture based on the first-order Langevin function (Eq. (1)) averaged out with a lognormal distribution of magnetic moments (Eq. (2)).

distribution plus improvement in crystallinity, the latter impacting in reducing the thickness of the so-called surface dead layer. Regardless the simplicity of the model picture represented by Eqs. (1) and (2) while fitting the experimental data shown in Fig. 2 (symbols), with no particle-particle interaction included in the model, a high-quality fitting was indeed achieved (solid lines in Fig. 2). Dipolar interaction among neighboring nanoparticles is expected to take place and thus should influence the magnetic behavior. However, in Eq. (1) the first-order Langevin function is averaged out by the distribution of magnetic moment (μ) and therefore particle-particle interaction, if in place, would be accounted for by the magnetic moment parameters (μ_0 and σ_μ). Actually, within the model picture herein applied for the analysis of magnetization μ_0 should be understood as the effective magnetic moment. From the viewpoint of nanomagnetic materials' characterization and their applications the approach described by Eqs. (1) and (2) is very much interesting as it provides reliable parameters (μ_0 and σ_μ) coming out from excellent curve fittings. This is indeed a very important point as it allows for instance the establishment of reliable protocols for calibrating magnetic properties of nanosized particles, which is extremely important in the emerging field of magnetic nanothermometry.³²

Figure 3 shows the average magnetic moment (μ_0) versus the third power of the crystallite size (D_{hkl})³, the former extracted from the fitting of the magnetization data whereas the latter obtained from the Rietveld refinement of the XRD data (see Table II), representing two independent and quite different experimental techniques. Impressively, the linear dependence revealed in Fig. 3 with the two parameters scaling as $\mu_0 \sim M_s^p D_{hkl}^3$. This means the nanoparticle's magnetization density (M_s^p) is constant, suggesting a core-shell model for all synthesized NPs (CO30, CO50, and CO95), with a crystalline core and an amorphous shell (dead layer), the first responding for the value of M_s^p . Considering the saturation magnetization of the NP's core matching with the bulk cobalt ferrite value

TABLE II. Crystallite size (D_{hkl}) extracted from the Rietveld refinement (Fig. 1) and average magnetic moment (μ_0), magnetic moment dispersity (σ_μ), and saturation magnetization (M_S) extracted from the M versus H fitting (Fig. 2).

Sample	D_{hkl} (nm)	μ_0 ($10^3 \mu_B$)	σ_μ	M_S (emu/g)
CO30	5.8 ± 0.7	2.6 ± 0.9	0.37 ± 0.07	37 ± 2
CO50	6.1 ± 0.5	11 ± 2	0.31 ± 0.05	60 ± 2
CO95	7.4 ± 0.2	16 ± 1	0.24 ± 0.02	66 ± 2

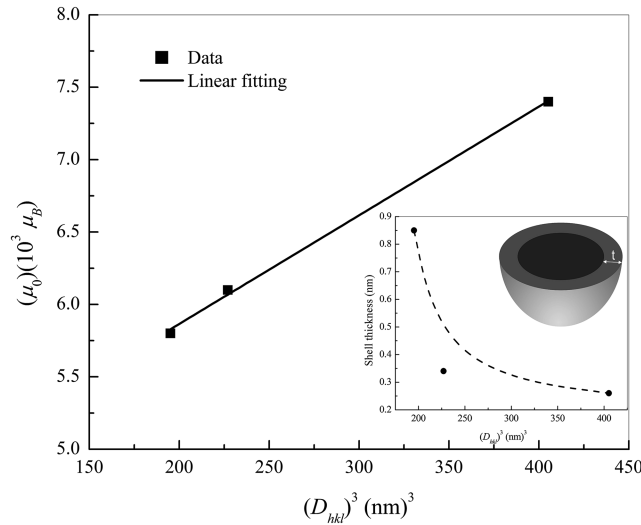


FIG. 3. Nanoparticle average magnetic moment versus third power of the crystallite size (solid squares are estimated values and the solid line is a linear fitting). The inset shows the reduction of the surface amorphous layer (dead layer) thickness in a core-shell-like structure (solid circles are estimated values and the dashed line is guide to the eyes).

($M_B = 80.8$ emu/g at 300 K) the thickness ($t = (D_p - D_{hkl})/2$) of the dead layer can be estimated (assuming homogeneous mass density and stoichiometry) for spherically-shaped NPs, with the physical size (D_p) equals to: $D_p = D_{hkl}(M_B/M_S)^{1/3}$. The inset of Fig. 3 shows the estimated thickness (symbols) of the dead layer as the crystallite size (D_{hkl}) increases while increasing the co-precipitation synthesis temperature. The systematic reduction of the dead layer thickness results in improvement of the crystalline and magnetic characteristics of the as-synthesized NPs, as quoted in Tables I and II. Importantly, the presence of the dead layer plus the room-temperature superparamagnetic behavior may account for the reduced particle-particle interaction, thus shining some light on the excellent curve-fitting (solid lines) of the data presented in Fig. 2 while using Eqs. (1) and (2).

CONCLUSIONS

In this study cobalt ferrite nanoparticles were synthesized by co-precipitation in alkaline medium at increasing temperatures in the range of 27 °C to 100 °C. Three prepared samples were structurally and magnetically characterized using x-ray diffraction (XRD) and room-temperature hysteresis cycle. Rietveld refinement of the XRD data showed that all produced samples were single-phased with diameters in the nanosized range and below 10 nm. The first-order Langevin function averaged out by the lognormal distribution function of magnetic moments provided excellent fitting of the magnetization versus magnetic field data. This approach resulted in high-quality fitting of magnetization data while allowing extract reliable average magnetic moment and magnetic moment dispersity values. The high-quality of the magnetization data may be of great help in establishing a robust calibration approach for magnetic nanothermometry. The co-precipitation protocol herein employed used very low stirring speed compensated by increasing the concentration of the sodium hydroxide solution in order to fabricate cobalt ferrite nanoparticles in the range of 5 to 10 nm in average size, revealing the potentiality of the approach for up-scaling production. Indeed, the model picture used to understand the experimental data is expected to contribute for the modulation of the morphological and magnetic properties of ferrite cobalt nanoparticles via core crystalline size and core shell size/shell thickness layer ratio.

ACKNOWLEDGMENTS

The authors thank Squid-UFSCAR_QD_MPMS3 do projeto FAPESP 09/54082-2 and the Brazilian agencies CNPq and FAPERO for the financial support.

- ¹ E. Tirosh, G. Shemer, and G. Markovich, *Chemistry of Materials* **18**, 465 (2006).
- ² Z. Iatridi, K. Vamvakidis, I. Tsougos, K. Vassiou, C. Dendrinou-Samara, and G. Bokias, *ACS Applied Materials and Interfaces* **8**, 35059 (2016).
- ³ H. Gu, K. Xu, Z. Yang, C. K. Chang, and B. Xu, *Chemical Communications* **34**, 4270 (2005).
- ⁴ U. Luders, A. Barthelemy, M. Bibes, K. Bouzehouane, S. Fusil, E. Jacquet, J. P. Contour, J. F. Bobo, J. Fontcuberta, and A. Fert, *Advanced Materials* **18**, 1733 (2006).
- ⁵ G. Baldi, D. Bonacchi, C. Innocenti, G. Lorenzi, and C. Sangregorio, *Journal of Magnetism and Magnetic Materials* **311**, 10 (2007).
- ⁶ A. T. Ngo, P. Bonville, and M. P. Pileni, *Journal of Applied Physics* **89**, 3370 (2001).
- ⁷ P. C. Morais, J. S. Santos, K. Skeff Neto, F. Pelegrini, and M. De Cuyper, *Journal Magnetism and Magnetic Materials* **293**, 526 (2005).
- ⁸ B. D. Cullity, *Introduction to magnetic materials* (Addison Wesley Publishing Company, 1972).
- ⁹ F. M. L. Oliveira, S. R. Avelino, M. T. A. Elói, P. P. Gravina, K. Skeff Neto, E. C. D. Lima, and P. C. Morais, *Journal of Non-Crystalline Solids* **352**, 3689 (2006).
- ¹⁰ B. M. Lacava, R. B. Azevedo, L. P. Silva, A. G. M. Lacava, K. Skeff Neto, N. Buske, A. F. Bakuzis, and P. C. Morais, *Applied Physics Letters* **77**, 1876 (2000).
- ¹¹ S. Zhang, D. Dong, Y. Sui, Z. Liu, H. Wang, Z. Qian, and W. Su, *Journal of Alloys and Compounds* **415**, 257 (2006).
- ¹² E. Tirosh, G. Shemer, and G. Markovich, *Chemistry of Materials* **18**, 465 (2006).
- ¹³ K. V. P. M. Shafi, A. Gedanken, R. Prozorov, and J. Balogh, *Chemistry of Materials* **10**, 3445 (1998).
- ¹⁴ Z. Huang and F. Tang, *Journal of Colloid and Interface Science* **281**, 432 (2005).
- ¹⁵ M. Rejandra, R. C. Pullar, A. K. Bhattacharya, D. Das, S. N. Chintalapudi, and C. K. Majumdar, *Journal of Magnetism and Magnetic Materials* **232**, 71 (2001).
- ¹⁶ K. J. Shea and D. A. Loy, *Chemistry of Materials* **13**, 3306 (2001).
- ¹⁷ N. Mouden and M. P. Pileni, *Chemistry of Materials* **8**, 1128 (1996).
- ¹⁸ Y. Li and C. W. Park, *Langmuir* **15**, 952 (1999).
- ¹⁹ K. El-Sayed, M. B. Mohamed, Sh. Hamdy, and S. S. Ata-Allah, *Journal of Magnetism and Magnetic Materials* **423**, 291 (2017).
- ²⁰ P. C. Morais, R. L. Santos, A. C. M. Pimenta, R. B. Azevedo, and E. C. D. Lima, *Thin Solid Films* **515**, 266 (2006).
- ²¹ A. Sathya, P. Guardia, R. Brescia, N. Silvestri, G. Pugliese, S. Nitti, L. Manna, and T. Pellegrino, *Chemistry of Materials* **28**, 1769 (2016).
- ²² D. Li, H. Yun, B. Diroll, V. V. T. Doan-nguyen, J. C. Kikkawa, and C. B. Murray, *Chemistry of Materials* **28**, 480 (2016).
- ²³ R. Massart, "Magnetic fluid and process for obtaining them," 4329241. US Patent (1982).
- ²⁴ C. N. Chinnasamy, M. Senoue, B. Jeyadevan, O. Perales-Perez, K. Shinoda, and K. Tohji, *Journal of Colloid and Interface Science* **263**, 80 (2003).
- ²⁵ Y. Kim, D. Kim, and C. S. Lee, *Physica B* **337**, 42 (2003).
- ²⁶ C. N. Chinnasamy, B. Jeyadevan, O. Perales-Perez, K. Shinoda, K. Tohji, and A. Kasuya, *IEEE Transactions on Magnetics* **38**, 2640 (2002).
- ²⁷ Z. B. Huang and F. Q. Tang, *Journal of Colloid and Interface Science* **281**, 432 (2005).
- ²⁸ H. M. Rietveld, *Journal of Applied Crystallography* **2**, 65 (1969).
- ²⁹ R. Safi, A. Ghasemi, and R. Shoja-Razavi, *Ceramics International* **42**, 17357 (2016).
- ³⁰ J. Langford, D. Louer, and P. Scardi, *Journal of Applied Crystallography* **33**, 964 (2000).
- ³¹ A. Le Bail, *Powder Diffraction* **19**, 249 (2004).
- ³² J. Zhong, W. Liu, L. Kong, and P. C. Morais, *Scientific Reports* **4**, 6338 (2014).